

## Article

# Operation Optimization of Thermal Management System of Deep Metal Mine Based on Heat Current Method and Prediction Model

Wenpu Wang<sup>1</sup>, Wei Shao<sup>1,2,\*</sup>, Shuo Wang<sup>1</sup>, Junling Liu<sup>1</sup>, Kun Shao<sup>2</sup> , Zhuoqun Cao<sup>2</sup>, Yu Liu<sup>1</sup> and Zheng Cui<sup>2,\*</sup>

<sup>1</sup> Institute of Thermal Science and Technology, Shandong University, Jinan 250061, China; wangwenpu@mail.sdu.edu.cn (W.W.); swang@mail.sdu.edu.cn (S.W.); junlingl2022@163.com (J.L.); liuyu2017@sdu.edu.cn (Y.L.)

<sup>2</sup> Shandong Institute of Advanced Technology, Jinan 250100, China; kun.shao@iat.cn (K.S.); zhuoqun.cao@iat.cn (Z.C.)

\* Correspondence: shao@sdu.edu.cn (W.S.); zhengc@sdu.edu.cn (Z.C.)

**Abstract:** With the increasing depth of metal mining, thermal damage has become a serious problem that restricts mining. The thermal management system of refrigeration and ventilation is an indispensable technology in the mining of deep metal mines, which plays a key role in improving the thermal and humid environment of mines. Optimizing the performance of refrigeration and ventilation systems to reduce energy consumption has become a focus of researchers' attention. Based on the heat current method, this research establishes the overall heat transfer and flow constraint model of the refrigeration and ventilation system, and proposes an iterative algorithm that combines the refrigerator energy consumption model and the artificial neural network model of heat exchangers. The Lagrange multiplier method is used to optimize the system with the goal of minimizing the total power consumption of the system. The results show that under 9.1 kW cooling load conditions, the total energy consumption of the system reduces by 16.5%, and the COP of the refrigerator increases by 11.6%. The optimization results provide significant guidance for the production and energy consumption reduction of the deep metal mines.

**Keywords:** heat current method; deep mine; operation optimization; Lagrange multiplier method; artificial neural network model (ANN)



**Citation:** Wang, W.; Shao, W.; Wang, S.; Liu, J.; Shao, K.; Cao, Z.; Liu, Y.; Cui, Z. Operation Optimization of Thermal Management System of Deep Metal Mine Based on Heat Current Method and Prediction Model. *Energies* **2023**, *16*, 6626. <https://doi.org/10.3390/en16186626>

Academic Editors: Ciro Aprea, Adrián Mota Babiloni, Rodrigo Llopis, Jaka Tušek, Angelo Maiorino, Andrej Žerovnik and Juan Manuel Belman-Flores

Received: 18 August 2023  
Revised: 10 September 2023  
Accepted: 13 September 2023  
Published: 14 September 2023



**Copyright:** © 2023 by the authors. Licensee MDPI, Basel, Switzerland. This article is an open access article distributed under the terms and conditions of the Creative Commons Attribution (CC BY) license (<https://creativecommons.org/licenses/by/4.0/>).

## 1. Introduction

The impact of high-temperature heat damage on the working efficiency and physical and mental health of workers is aggravated with the increase in mining depth [1]. It is necessary to improve the working environment of deep metal mines by artificial refrigeration and ventilation [2]. Up to now, there are three main artificial cooling measures at home and abroad, namely: central air conditioning cooling technology, ice cooling technology, and water cooling technology [3]. These technologies each have their own advantages and disadvantages. The central air conditioning cooling technology has a long application time and high efficiency, but the system is complex and has high construction costs, and there is a large amount of extended cooling capacity loss. Ice cooling technology has low cooling capacity loss, low working fluid flow rate, and good cooling effect, but with high initial investment, complex system, easy blockage, and high operation and maintenance costs. The water source heat pump system uses mine water as a cold source, which has low energy consumption, low investment, low operating cost, and can recover residual heat from mine water. However, its refrigeration efficiency is low, and it has high requirements for mine water volume. There are also some applications of other cooling technologies. He et al. [4] proposed a HEMS (high-temperature exchange machinery system) technology

for extracting cold energy from mine inflow and successfully applied it. Niu et al. [5] designed a comprehensive system for mine cooling and thermal energy utilization that integrates water source heat pump and central air conditioning technology, achieving a significant reduction in equipment investment and operating costs.

The combination of different technologies can achieve better results. However, due to various reasons, there is currently no unified standard and specification in the industry for the design of deep mine ventilation and refrigeration systems. In the system design process, it is necessary to fully utilize existing resources based on the actual situation of the mine (such as return, inlet water, etc.), turn disadvantages into advantages, and reasonably select and design suitable, efficient, and economical refrigeration and ventilation systems according to local conditions.

The refrigeration and ventilation systems consume a large amount of energy during operation. It is an important issue to make the system meet the refrigeration demand under the most economical operating conditions. The optimization of the mine refrigeration system has great potential to reduce operating costs, and it is an important component of ensuring safe working conditions underground. Systems typically have the characteristics of numerous components and complex structures, and researchers need to consider the heat transfer and thermal relationships between different components. The optimization goal can be to minimize the total investment or operating costs of the system.

At present, there are many research studies on the modeling and operation optimization of thermal management systems. Li et al. [6] established a dynamic model of a three-wheel air cycle refrigeration system and provided transient performance data under various operating conditions. Sun et al. [7] used methods such as semi-thermodynamic modeling, regional modeling, and distributed modeling to model the refrigeration system. Li et al. [8] proposed a numerical model for a variable displacement VCR system based on the heat exchanger model and the compressor model. Tirmizi et al. [9] carried out detailed mathematical modeling for each component of the central chilled water system. Huh et al. [10] optimized the humidity and temperature control of the air conditioning system using a theoretical/empirical combination modeling strategy. Baakeem et al. [11] modeled a multi-stage steam compression refrigeration system. Zhao et al. [12] proposed an optimization strategy for vapor compression refrigeration based on the model. Nunes et al. [13] optimized a vapor compression refrigeration system by establishing a dynamic mathematical model. Some researchers use artificial neural network technology (ANN) for modeling and optimization [14–17].

Current optimization research often focuses on the optimization analysis of components, while local optima do not necessarily represent system optima. How to establish global connections between the system and its components from the perspective of the system as a whole, and conduct overall system analysis and optimization for different optimization objectives, is a problem worth studying. The problem with the above method lies in the presence of many intermediate variables and complex solutions. The nonlinearity of the system gradually increases as the complexity of the thermal management system increases. Efficient and concise modeling and simulation methods are essential for the optimization and analysis of the thermal management system. The heat current method for modeling complex thermal systems proposed by Chen et al. [18] provides great convenience for system optimization and analysis. The basic thought of the heat current method is to use the electrical analogy method to establish the equivalent thermal circuits and the global energy transfer and conversion law of the system, and then optimize the model with Lagrange and other algorithms [18]. The heat current method has been successfully applied in various fields of optimization of thermal systems, such as organic Rankine cycle [19], steam power generation systems [20], integrated ground source heat pumps and solar PVT systems [21], and heat transfer systems [22], etc. Based on the heat current method, Li et al. [23] optimized the aircraft refrigeration system.

The optimization concept of the heat current method establishes a direct connection between the structural parameters, demand parameters, and operational parameters of

the thermal system, providing convenience and a foundation for global analysis of the system. This method has been developed in the process of research and application. In complex systems, the flow characteristics have an appreciable effect on system performance. Wang et al. [24] analyzed the flow characteristics of the system, established overall driving force resistance constraints of the system, and combined the heat current method to achieve collaborative optimization of the heat transfer and flow characteristics of the thermal management system. At the same time, the heat current method has proved that it can be combined with other methods to optimize the thermal system, such as the Pareto optimization method [19] and computational fluid dynamics (CFD) [25], to provide more reliable results. There are some complex issues in the traditional optimization process. There is a phase change process during the operation of the refrigerator, which increases the difficulty of theoretical analysis and model calculation. Additionally, the thermal conductivity ( $kA$ ) of heat exchangers is also a key parameter that describes its heat transfer capacity, which is only related to the structure of the heat exchanger and the flow rate of fluids. The thermal conductivity of the heat exchanger is only determined by the fluid flow rate on the cold and hot sides in a fixed heat exchange network, and the relationship between them is complex and nonlinear.

In this paper, a thermal management experimental platform for refrigeration and ventilation of metal deep mines is built. Firstly, this research establishes an equivalent thermal resistance model and flow resistance model of the system based on the heat current method. This article proposes a new iterative algorithm to address the problems in heat transfer optimization by establishing energy consumption models for refrigerators and thermal conductivity models for heat exchangers. In order to minimize the total energy consumption of the system under certain thermal load conditions, this paper uses the Lagrange multiplier method and a new iterative algorithm for optimization calculation based on the overall heat transfer and flow constraints of the system. Finally, the optimization results are verified and discussed through experiments. This modeling and optimization method has important guiding significance for the energy-saving of simulation systems and mine cooling systems.

## 2. Introduction of the Refrigeration and Ventilation System Experimental Platform

### 2.1. System Description and Thermal Analysis

In order to solve the problem of thermal damage caused by the increase in thermal load and ventilation limit in the production process of deep mines, it is necessary to design an efficient and energy-saving refrigeration and ventilation system for deep mines. According to the actual situation, the air-cooling tower can be placed in the return air shaft and the refrigeration system can be arranged underground. This can fully utilize the wind energy from the return air shaft, reducing the pipeline materials. At the same time, an intermediate elastic tube bundle heat exchanger is designed, which can reduce the pressure of the refrigerator and reduce the corrosion of water on the heat exchanger. Based on this idea, an experimental platform for the refrigeration and ventilation system in deep metal mines was built. Figure 1 shows the on-site photos and schematic diagram of key components of the experimental platform.

Figure 2 displays the structure diagram of the experimental platform of the refrigeration and ventilation system. This system is divided into three parts: stope cooling part, refrigerator, and system cooling part. According to the perspective of the circuit, the system can be divided into an air-cooling tower cooling circuit, intermediate cooling circuit, chilled water circuit, and mining site cooling air pipeline. Water is used as the circulating working medium in all circulating circuits. Under normal temperature and pressure, the constant pressure-specific heat capacity of water is  $4200 \text{ J}/(\text{kg K})$  and the density is  $1000 \text{ kg}/\text{m}^3$ . The refrigerator uses R134 as refrigerant, with a pressure of  $0.47 \text{ Mpa}$ , a constant pressure specific heat capacity of  $1304 \text{ J}/(\text{kg K})$ , and a density of  $1100 \text{ kg}/\text{m}^3$  when saturated with liquid ( $300 \text{ K} \pm 10 \text{ K}$ ). The medium of the air cooling pipeline

is air, the constant pressure-specific heat capacity of air is 1005 J/(kg K) and the density is 1.293 kg/m<sup>3</sup> [26].



Figure 1. Picture of the refrigeration and ventilation system experimental platform.

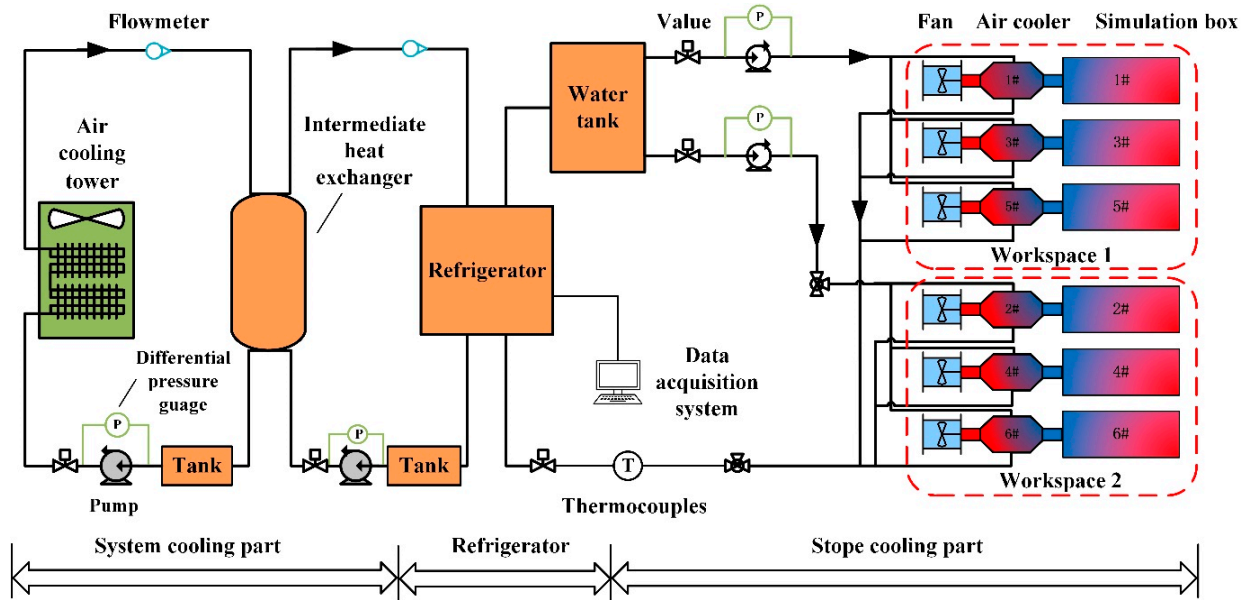


Figure 2. Structure diagram of the cooling and ventilation system.

The stope cooling part is primarily used to cool six (#1–#6) mine stope environment simulation boxes by conveying cold air. It mainly includes a chilled water circuit (CHWC) and six air cooling lines (CAL). Hot air exchanges heat with chilled water conveyed by the pump in the air cooler. The fan conveys the air at a lower temperature to the simulation box. As the temperature of chilled water rises, it returns to the water side of the evaporator of the refrigerator and completes the cycle. The heat transfer relationship involved in air coolers can be expressed as

$$Q_{aaj} = m_{aaj}c_{p,a}(T_{aaj,i} - T_{aaj,o}), j = 1, 2, \dots, 6 \quad (1)$$

$$Q_{awj} = m_{awj}c_{p,w}(T_{awj,o} - T_{awj,i}), j = 1, 2, \dots, 6 \quad (2)$$

where  $Q_{awj}$  and  $Q_{aaj}$ , respectively, represent the heat transfer rate on the cold and hot sides of the air cooler.  $m_{aaj}$  and  $m_{awj}$  represent the mass flow rate of the airflow and water flow of the  $j$ -th air cooler,  $c_{p,a}$  and  $c_{p,w}$  represent the specific heat capacity of air and water, and  $T_{aaj,i}$  and  $T_{aaj,o}$  are the inlet and outlet temperatures of hot air.  $T_{awj,i}$  and  $T_{awj,o}$  are the inlet and outlet temperatures of chilled water. According to the law of conservation of energy,  $Q_{aaj}$  should equal to  $Q_{awj}$ .

The refrigerator includes an evaporator, expansion valve, condenser, compressor, and other components, which are mainly used to produce chilled water. The expressions for the heat transfer rate of water on both sides of the refrigerator are

$$Q_{ch} = m_{ch}c_{p,w}(T_{chwr} - T_{chws}) \quad (3)$$

$$Q_c = m_{cw}c_{p,w}(T_{cw,o} - T_{cw,i}) \quad (4)$$

where  $Q_{ch}$  is the refrigerating capacity of the refrigerator,  $Q_c$  is the heat transfer rate of the water side of condenser,  $m_{ch}$  is the mass flow rate of the chilled water,  $m_{cw}$  is the mass flow rate of cooling water of condenser,  $T_{chws}$  and  $T_{chwr}$  are the supply and return temperatures of chilled water, and  $T_{cw,i}$  and  $T_{cw,o}$  are the inlet and outlet temperatures of cooling water of the condenser.  $Q_{ch}$  equals the total heat transfer rate of the air coolers,  $Q_c$  is equal to the sum of  $Q_{ch}$  and the power consumption of the refrigerator ( $P_{re}$ ), and also the total heat transfer rate of the system, which can be expressed as

$$Q_{ch} = \sum_{j=1}^6 Q_{aj}, j = 1, 2, \dots, 6 \quad (5)$$

$$Q_c = Q_{ch} + P_{re} \quad (6)$$

where  $Q_{aj}$  is the heat transfer rate of the  $j$ -th air cooler.

The coefficient of performance of the refrigerator ( $COP$ ) is determined by the following relation

$$COP = \frac{Q_{ch}}{P_{re}} \quad (7)$$

The system cooling part mainly includes two cooling water circuits: the intermediate cooling circuit ( $ICC$ ) and the air-cooling tower circuit ( $ACTC$ ). The intermediate heat exchanger is used to absorb the heat released by the condenser and then transfer the heat to the air-cooling tower, which exchanges heat with the atmosphere and carries the heat outdoors. The heat transfer rate in this section is

$$Q_{mh} = m_m c_{p,w} (T_{mh,i} - T_{mh,o}) \quad (8)$$

$$Q_{mc} = m_{ct} c_{p,w} (T_{mc,o} - T_{mc,i}) \quad (9)$$

where  $Q_{mh}$  and  $Q_{mc}$  are the heat transfer rate of the cold water side and hot water side of the intermediate heat exchanger,  $m_m$  is the mass flow rate of  $ICC$ ,  $T_{mh,i}$  and  $T_{mh,o}$  are the inlet and outlet temperatures of the hot side.  $m_{ct}$  is the mass flow rate of  $ACTC$ ,  $T_{mc,i}$  and  $T_{mc,o}$  are the inlet and outlet temperatures of the cold side. The heat transfer rate of the intermediate heat exchanger is equal to  $Q_c$ , which is

$$Q_{mh} = Q_{mc} = Q_c \quad (10)$$

Variable frequency pumps and fans are used to deliver water and air in each circuit. The flowmeters are used to measure the mass flow rate of water, and the difference pressure gauges are used to measure the pressure differences. The thermocouples are used to measure the temperatures. The data acquisition system records and stores the experimental data. Table 1 shows the main measuring instruments and their accuracy.

**Table 1.** Information of measuring instrument.

Measuring Instrument	Type	Range	Accuracy
Thermocouple	TT-T-24-SLE-1000	−267–150 °C	0.4%
Flowmeter	AXF050G	0.3–10 m/s	0.5%
Differential pressure gauge	EJA110E	0–500 kPa	0.055%
Anemometer	WD-400	0–20 m/s	3%

## 2.2. Uncertainty Analysis

The uncertainty test of the experiment is a guarantee of the credibility of the experiment. Supposing the function  $R$  contains  $n$  mutually independent variables,  $x_1, x_2, \dots, x_n$ ,  $W_{x_1}, W_{x_2}, \dots, W_{x_n}$  is the uncertainty corresponding to each variable. So, the uncertainty of function  $R$  can be determined by

$$W_R = \sqrt{\left(\frac{\partial R}{\partial x_1} W_{x_1}\right)^2 + \left(\frac{\partial R}{\partial x_2} W_{x_2}\right)^2 + \dots + \left(\frac{\partial R}{\partial x_n} W_{x_n}\right)^2} \quad (11)$$

The heat transfer rate is indirectly measured data. Table 2 shows the uncertainty of the experiment data.

**Table 2.** The uncertainty of the experiment data.

Heat Transfer Rate (W)	Uncertainty (P = 68.3%)
Hot side of the air cooler	6.7%
Cold side of the air cooler	5.6%
Refrigerating capacity	5.8%
Cooling water side of condenser	9.7%
Hot side of intermediate heat exchanger	5.7%
Cold side of intermediate heat exchanger	9.7%

## 3. Theoretical Analysis and Constraints

This chapter focuses on the modeling and optimization of the built refrigeration and ventilation system experimental platform. Firstly, a comprehensive heat transfer model of the system was established based on the heat current method, without introducing other intermediate variables. By analyzing the fluid network of the system, the characteristic parameters of the power components and pipeline network are identified, and an overall flow resistance model based on driving force resistance constraints is established. In order to solve the complex analysis problem of fixed thermal conductivity of refrigerators and heat exchangers in traditional optimization analysis, response surface modeling and artificial neural network modeling methods are used in this section to model the refrigerant energy consumption and thermal conductivity of heat exchangers using experimental data. Based on the overall heat transfer flow model of the system, aiming at the minimum energy consumption of the system, the Lagrange multiplier method is used to optimize the system, combined with the iterative algorithm of energy consumption and thermal conductivity update, and the optimization results are analyzed through experiments. The optimization results show that the total power consumption of power components has been reduced by 39.1%, the power consumption of the refrigerator has been reduced by 11.4%, and the total energy consumption of the system has been reduced by 16.5%. The comparison between the optimization value and the experimental value shows that the maximum deviation of heat exchange is 8.8%, which is within the allowable range of error.

### 3.1. Heat Current Model of System

Taking the heat transfer process of a counter-current heat exchanger as an example, this section briefly explains the modeling principle of the heat current method, Figure 3 shows the heat transfer  $Q$  from a hot fluid to a cold fluid.

Assuming that the two fluids are single-phase and their physical properties remain unchanged, the energy conservation equation involved in the heat exchanger is:

$$Q = G_h(T_{h,i} - T_{h,o}) = G_c(T_{c,o} - T_{c,i}) \quad (12)$$

where  $T_{h,i}$  and  $T_{h,o}$  are the inlet and outlet temperatures of the hot side fluid,  $T_{c,i}$  and  $T_{c,o}$  are the inlet and outlet temperatures of the cold side fluid, respectively, and  $G$  represents the thermal capacity flow of the fluid, and its expression is

$$G = mc_p \tag{13}$$

where  $m$  is the mass flow rate of the fluid, and  $c_p$  is the specific heat capacity of the fluid at constant pressure.

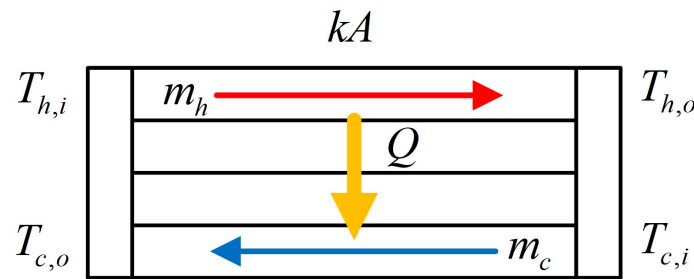


Figure 3. Heat transfer principle diagram of counter-current heat exchanger.

Qun Chen et al. [27] derived the heat transfer relationship of a heat exchanger through the energy conservation equation and thermoelectric analogy. They compared the inlet temperature difference to thermal potential,  $R$  to thermal resistance, and  $Q$  to heat flow. Figure 4 shows the heat current model of the heat exchanger.

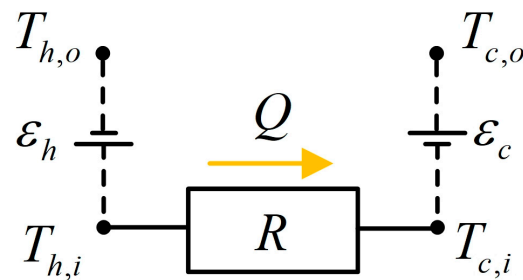


Figure 4. Heat current model diagram of heat exchanger.

The heat transfer relationship involved can be expressed as:

$$Q = \frac{T_{h,i} - T_{c,i}}{R} \tag{14}$$

The expression for the thermal resistance  $R$  derived based on the inlet temperature difference is

$$R = \frac{G_h e^{a_c} - G_c e^{a_h}}{G_h G_c (e^{a_c} - e^{a_h})} \tag{15}$$

where  $G_c$  and  $G_h$ , respectively, represent the thermal capacity flow of cold and hot fluids, while  $a_c$  and  $a_h$ , respectively, represent the ratio of the thermal conductivity ( $kA$ ) of the heat exchanger to the thermal capacity flow of cold and hot fluids. The combination of heat current models for different heat exchangers can establish a heat current network model.

Based on the above analysis, the equivalent thermal resistance network diagram of the system established based on the heat current method [28] is shown in Figure 5.

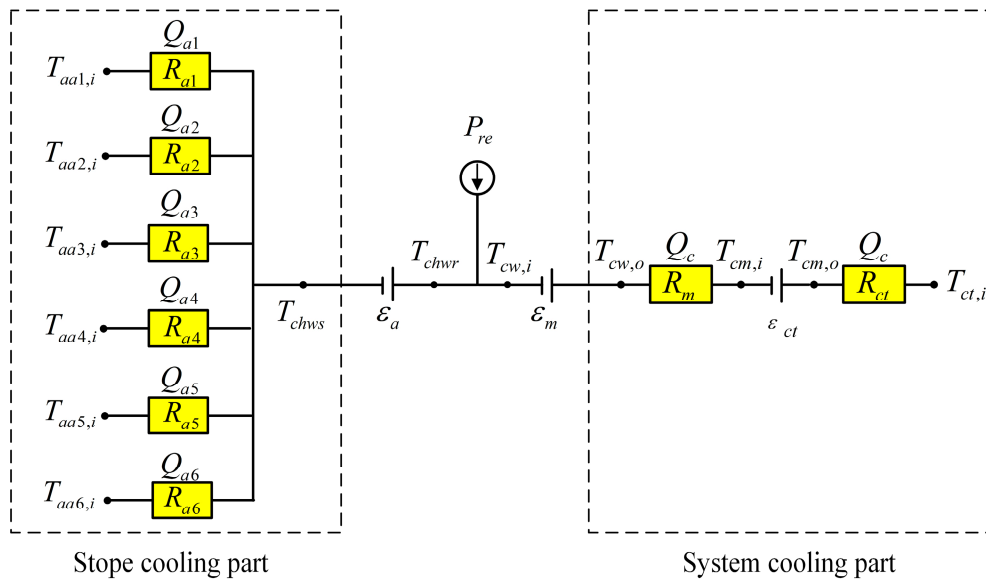


Figure 5. Thermal resistance network diagram.

Firstly, the thermoelectric analogy method and Kirchhoff’s current voltage law are used to analyze the stope cooling part, the heat transfer constraints of this part are established as follows:

$$T_{aa,j} - T_{chws} = R_{aj}Q_{aj}, j = 1, 2, \dots, 6 \tag{16}$$

where  $\epsilon_a$  represents the equivalent thermal potential difference, and its expression is

$$\epsilon_a = \frac{Q_{ch}}{G_{ch}} \tag{17}$$

where  $G_{ch}$  is the heat capacity flow of chilled water, there is

$$G_{ch} = m_{ch}c_{p,w} \tag{18}$$

$R_{aj}$  is the equivalent thermal resistance of the  $j$ -th air cooler. Since the air cooler is a cross-flow heat exchanger, its expression is:

$$R_{aj} = \frac{G_{aa,j}e^{NTU_{awj}} - G_{aw,j}e^{NTU_{aa,j}}}{G_{aa,j}G_{aw,j}(e^{NTU_{awj}} - e^{NTU_{aa,j}})}, j = 1, 2, \dots, 6 \tag{19}$$

where  $G_{aa,j}$  represents the heat capacity flow of the airflow of the  $j$ -th air cooler.  $G_{aw,j}$  is the heat capacity flow of the water flow of the  $j$ -th air cooler.  $NTU_{aa,j}$  and  $NTU_{aw,j}$  are dimensionless parameters. Their expressions are:

$$G_{aw,j} = m_{aw,j}c_{p,w}, j = 1, 2, \dots, 6 \tag{20}$$

$$G_{aa,j} = m_{aa,j}c_{p,a}, j = 1, 2, \dots, 6 \tag{21}$$

$$NTU_{aw,j} = \frac{\varphi_{aj}(kA)_{aj}}{G_{aw,j}}, j = 1, 2, \dots, 6 \tag{22}$$

$$NTU_{aa,j} = \frac{\varphi_{aj}(kA)_{aj}}{G_{aa,j}}, j = 1, 2, \dots, 6 \tag{23}$$

where  $(kA)_{aj}$  is the thermal conductance of the  $j$ -th air cooler.  $\varphi_{aj}$  is the correction factor of the thermal conductivity of the cross-flow heat exchanger. The calculation of  $\varphi_{aj}$  requires the introduction of two dimensionless coefficients  $P_{aj}$  and  $U_{aj}$  [29]. The expressions are as follows:

$$\varphi_{aj} = \frac{\ln[(1 - U_{aj}P_{aj}) / (1 - P_{aj})]}{(1 - 1/U_{aj}) \ln[1 + U_{aj} \ln(1 - P_{aj})]}, \quad j = 1, 2, \dots, 6 \quad (24)$$

$$P_{aj} = \frac{T_{awj,o} - T_{awj,i}}{T_{aa,j,i} - T_{awj,i}}, \quad j = 1, 2, \dots, 6 \quad (25)$$

$$U_{aj} = \frac{T_{aa,j,i} - T_{aa,j,o}}{T_{awj,o} - T_{awj,i}}, \quad j = 1, 2, \dots, 6 \quad (26)$$

The heat transfer constraints of the system heat removal part are established as follows:

$$T_{ct,i} - T_{cw,o} = Q_c R_{ct} - \varepsilon_{ct} + Q_c R_m \quad (27)$$

where  $T_{ct,i}$  is the inlet air temperature of the air-cooling tower, i.e., the atmospheric temperature.  $\varepsilon_m$  and  $\varepsilon_{ct}$  represent the equivalent thermal potential difference, which can be expressed as

$$\varepsilon_m = \frac{Q_c}{G_m} \quad (28)$$

$$\varepsilon_{ct} = \frac{Q_c}{G_{ct}} \quad (29)$$

where  $G_m$  represents the heat capacity flow of the water flow of ICC.  $G_{ct}$  represents the heat capacity flow of the water flow of ACTC. They can be represented as:

$$G_m = m_m c_{p,w} \quad (30)$$

$$G_{ct} = m_{ct} c_{p,w} \quad (31)$$

where  $R_m$  is the equivalent thermal resistance of the intermediate heat exchanger.  $R_{ct}$  is the equivalent thermal resistance of the air-cooling tower. The cold side of the air-cooling tower is assumed to have infinite heat capacity. After the simplification and derivation of the thermal resistance, their expressions are

$$R_m = \frac{G_m e^{a_{mc}} - G_{ct} e^{a_{mh}}}{G_m G_{ct} (e^{a_{mc}} - e^{a_{mh}})} \quad (32)$$

$$R_{ct} = \frac{e^{a_{ct}}}{G_{ct} (e^{a_{ct}} - 1)} \quad (33)$$

where  $a_{mc}$ ,  $a_{mh}$ , and  $a_{ct}$  are dimensionless parameters, which are determined by the following relations:

$$a_{mc} = \frac{kA_m}{G_{ct}} \quad (34)$$

$$a_{mh} = \frac{kA_m}{G_m} \quad (35)$$

$$a_{ct} = \frac{kA_{ct}}{G_{ct}} \quad (36)$$

where  $(kA)_m$  is the thermal conductance of the intermediate heat exchanger.  $(kA)_{ct}$  is the thermal conductance of the air-cooling tower.

### 3.2. Flow Resistance Constraint Model

The variable frequency pumps and fans provide power for the fluid cycling, and their model can be expressed as [30]:

$$H = a_0\omega^2 + a_1\omega m + a_2m^2 \tag{37}$$

where  $H$  is the pressure head,  $\omega$  is the operating frequency.  $A_0$ ,  $a_1$ , and  $a_2$  are the characteristic parameters, which can be obtained through fitting and regression of experimental data.  $m$  is the mass flow rate. Table 3 shows the characteristic parameters and maximum deviation of the power components obtained through experiments. The maximum error is within the allowable range.

**Table 3.** Characteristic parameters and maximum deviation of the power components.

Power Components	$a_0$	$a_1$	$a_2$	$R^2$	Maximum Deviation
No. 1 fan	0.00993	−0.14186	−186.506	0.965	6.6%
No. 2 fan	0.00705	1.26833	−508.908	0.999	5.0%
No. 3 fan	0.01541	1.27508	−421.1733	0.997	4.3%
No. 4 fan	0.01616	−2.62011	247.85273	0.993	2.7%
No. 5 fan	0.00986	0.19266	−178.1779	0.984	3.1%
No. 6 fan	0.00896	1.64393	−589.0558	0.929	3.5%
No. 1 CHWC pump	0.0118	0.09784	−16.27054	0.991	6.1%
No. 3 CHWC pump	0.01243	0.02437	−12.02754	0.992	5.1%
ICC pump	0.01074	0.02506	−2.40889	0.995	4.7%
ACTC pump	0.00657	0.26856	−5.6721	0.992	5.4%

Next, the resistance network of the system is analyzed. Based on the pipe network structure, the pipe network resistance diagram shown in Figure 6 is established [31].

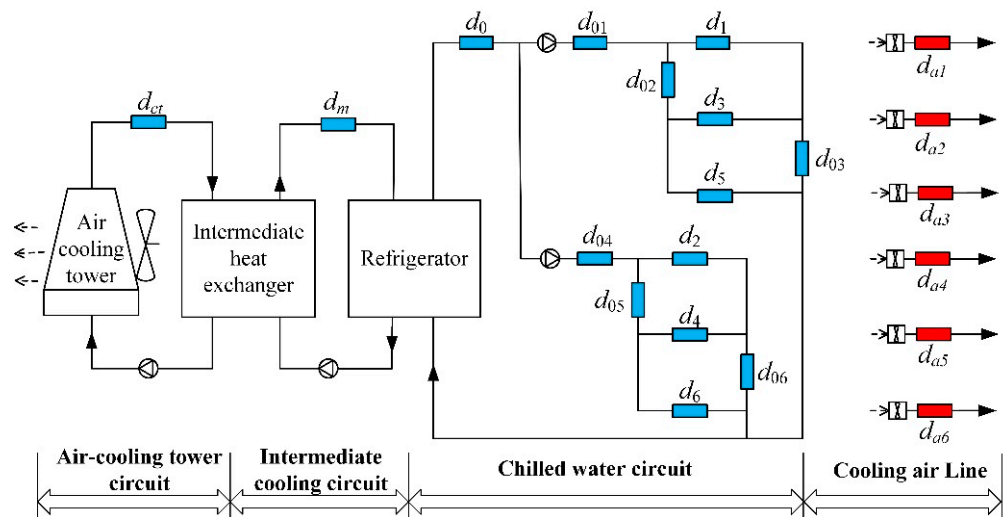


**Figure 6.** Schematic diagram of system flow resistance network.

For a fixed pipe network with an unchanged local structure, assuming that the Darcy coefficient does not change much when the range of working medium flow rate is small, the pressure head generated by the pipe network flow can be expressed as [32]:

$$H = d_0m^2 \tag{38}$$

where  $d_0$  is the dynamic head coefficient of the pipe network. For a fixed pipe network, it is the property parameter of the pipe network.

Firstly, for simple structured *CAL*, *ICC*, and *ACTC*, the characteristic parameters can be directly fitted by measuring the pressure differences corresponding to different mass flow rates. Table 4 shows the pipe network property parameters and  $R^2$ .

**Table 4.** Pipe network characteristic parameters.

Parameters	$d_0$ ( $\text{m}\cdot\text{s}^2/\text{kg}^2$ )	$R^2$
No. 1 airline	482.8	0.952
No. 2 airline	437.1	0.995
No. 3 airline	1054.8	0.998
No. 4 airline	727.8	0.994
No. 5 airline	500.9	0.967
No. 6 airline	1210.6	0.956
ICC	10.1	0.999
ACTC	10.5	0.997

*CHWC* includes a complex process structure for series/parallel heat exchange systems, with multiple branch pipe sections and multiple different flow parameters. Due to the different coefficients of each branch, experimental steps were set up to measure the mass flow rates of each branch and the pressure differences at both ends of the variable frequency pump.

- (1) Keeping the circuit fully open, adjusting the valve to parallel the six heat exchangers, and measuring the flow rate of each branch and the two ends of the pump under the condition of 100% frequency operation of the pump. The constraint relationships are as follows:

$$\begin{aligned}
 H_c &= d_0 m_0^2 + d_{01} m_{01}^2 + d_1 m_{aw1}^2 + d_{03} m_{03}^2 \\
 &= d_0 m_0^2 + d_{01} m_{01}^2 + d_{02} m_{02}^2 + d_3 m_{aw3}^2 + d_{03} m_{03}^2 \\
 &= d_0 m_0^2 + d_{01} m_{01}^2 + d_{02} m_{02}^2 + d_5 m_{aw5}^2 \\
 &= d_0 m_0^2 + d_{04} m_{04}^2 + d_2 m_{aw2}^2 + d_{06} m_{06}^2 \\
 &= d_0 m_0^2 + d_{04} m_{04}^2 + d_{05} m_{05}^2 + d_4 m_{aw4}^2 + d_{06} m_{06}^2 \\
 &= d_0 m_0^2 + d_{04} m_{04}^2 + d_{05} m_{05}^2 + d_6 m_{aw6}^2
 \end{aligned} \tag{39}$$

- (2) Operating the three heat exchangers in parallel in the first branch and closing the valves in the second branch, there are the following constraints:

$$\begin{aligned}
 H_{c1} &= (d_0 + d_{01}) m_0^2 + d_1 m_{aw1}^2 + d_{03} m_{03}^2 \\
 &= (d_0 + d_{01}) m_0^2 + d_{02} m_{02}^2 + d_3 m_{aw3}^2 + d_{03} m_{03}^2 \\
 &= (d_0 + d_{01}) m_0^2 + d_{02} m_{02}^2 + d_5 m_{aw5}^2
 \end{aligned} \tag{40}$$

- (3) Similarly, closing the first branch, and the constraint for the third branch is

$$\begin{aligned}
 H_{c3} &= (d_0 + d_{04}) m_0^2 + d_2 m_{aw2}^2 + d_{06} m_{06}^2 \\
 &= (d_0 + d_{04}) m_0^2 + d_{05} m_{05}^2 + d_4 m_{aw4}^2 + d_{06} m_{06}^2 \\
 &= (d_0 + d_{04}) m_0^2 + d_{05} m_{05}^2 + d_6 m_{aw6}^2
 \end{aligned} \tag{41}$$

- (4) Finally, only one branch is opened at a time, and its constraint can be written as

$$H_1 = (d_0 + d_{01} + d_1 + d_{03}) m_{aw1}^2 \tag{42}$$

$$H_2 = (d_0 + d_{04} + d_2 + d_{06}) m_{aw2}^2 \tag{43}$$

$$H_3 = (d_0 + d_{01} + d_{02} + d_3 + d_{03}) m_{aw3}^2 \tag{44}$$

$$H_4 = (d_0 + d_{04} + d_{05} + d_4 + d_{06}) m_{aw4}^2 \tag{45}$$

$$H_5 = (d_0 + d_{01} + d_{02} + d_5)m_{aw5}^2 \tag{46}$$

$$H_6 = (d_0 + d_{04} + d_{05} + d_6)m_{aw6}^2 \tag{47}$$

where  $d_0, d_{01}, d_{02}, d_{03}, d_{04}, d_{05}, d_{06}, d_1, d_2, d_3, d_4, d_5,$  and  $d_6$  are pipe network characteristic parameters.  $H_c, H_{c1}, H_{c3}, H_1, H_2, H_3, H_4, H_5,$  and  $H_6$  are the pressure heads of each branch.  $M_0, m_{01}, m_{02}, m_{03}, m_{04}, m_{05},$  and  $m_{06}$  are mass flow rates of each branch, which is

$$m_0 = m_{aw1} + m_{aw2} + m_{aw3} + m_{aw4} + m_{aw5} + m_{aw6} \tag{48}$$

$$m_{01} = m_{aw1} + m_{aw3} + m_{aw5} \tag{49}$$

$$m_{02} = m_{aw3} + m_{aw5} \tag{50}$$

$$m_{03} = m_{aw1} + m_{aw3} \tag{51}$$

$$m_{04} = m_{aw2} + m_{aw4} + m_{aw6} \tag{52}$$

$$m_{05} = m_{aw4} + m_{aw6} \tag{53}$$

$$m_0 = m_{aw2} + m_{aw4} \tag{54}$$

Table 5 shows the pipe network characteristic parameters obtained by fitting experimental data. The maximum error between the experimental value and the fitting value is 6.3%.

**Table 5.** Pipe network properties parameters.

Item	$d_0$	$d_{01}$	$d_{02}$	$d_{03}$	$d_{04}$	$d_{05}$	$d_{06}$
value	84.62	94.1	41.02	-1.994	78.2	-0.8533	41.27
Item	$d_1$	$d_2$	$d_3$	$d_4$	$d_5$	$d_6$	
value	91.38	47.5	-4.038	58.45	5.695	72.43	

When the system operates stably, the driving force provided by the power components should be equal to the flow resistance in the pipe network, and this relationship can be expressed as

$$a_{0,aj}\omega_{aa_j}^2 + a_{1,aj}\omega_{aa_j}m_{aa_j} + a_{2,aj}m_{aa_j}^2 = d_{aj}m_{aa_j}^2, j = 1, 2, \dots, 6 \tag{55}$$

$$a_{0,ch1}\omega_{ch1}^2 + a_{1,ch1}\omega_{ch1}m_{01} + a_{2,ch1}m_{01}^2 = d_0m_0^2 + d_{01}m_{01}^2 + d_1m_{aw1}^2 + d_{03}m_{03}^2 \tag{56}$$

$$a_{0,ch3}\omega_{ch3}^2 + a_{1,ch3}\omega_{ch3}m_{04} + a_{2,ch3}m_{04}^2 = d_0m_0^2 + d_{04}m_{04}^2 + d_2m_{aw2}^2 + d_{06}m_{06}^2 \tag{57}$$

$$a_{0,ct}\omega_{ct}^2 + a_{1,ct}\omega_{ct}m_{ct} + a_{2,ct}m_{ct}^2 = d_{ct}m_{ct}^2 \tag{58}$$

$$a_{0,m}\omega_m^2 + a_{1,m}\omega_m m_m + a_{2,m}m_m^2 = d_m m_m^2 \tag{59}$$

where  $a_{0,aj}, a_{1,aj},$  and  $a_{2,aj}$  are characteristic parameters of the  $j$ -th ACL fan,  $\omega_{aa_j}$  is the frequency of the  $j$ -th ACL fan,  $d_{aj}$  is the characteristic parameter of the  $j$ -th ACL.  $a_{0,ch1}, a_{1,ch1},$  and  $a_{2,ch1}$  are characteristic parameters of the No. 1 CHWC pump,  $\omega_{ch1}$  is the frequency of No.1 CHWC pump.  $a_{0,ch3}, a_{1,ch3},$  and  $a_{2,ch3}$  are characteristic parameters of No. 3 CHWC pump,  $\omega_{ch3}$  is the frequency of No. 3 CHWC pump.  $a_{0,ct}, a_{1,ct},$  and  $a_{2,ct}$  are characteristic parameters of the ACTC pump,  $\omega_{ct}$  is the frequency of the ACTC

pump, and  $d_{ct}$  is the characteristic parameter of the ACTC pump.  $a_{0,m}$ ,  $a_{1,m}$  and  $a_{2,m}$  are characteristic parameters of the ICC pump,  $\omega_m$  is the frequency of the ICC pump, and  $d_{ct}$  is the characteristic parameter of the ICC pump. At this point, the flow resistance model of the system has been derived.

### 3.3. Energy Consumption Model of the Refrigerator

The performance characteristics of the refrigerator under different operating conditions can usually be described in the form of a quadratic function [33]. The energy consumption of the refrigerator is mainly determined by its refrigerating capacity and is also related to the temperature difference between the chilled water supply and the cooling water outlet. So, the energy consumption of a refrigerator can be expressed as:

$$P_{re} = a_0 + a_1(T_{cw,o} - T_{chws}) + a_2(T_{cw,o} - T_{chws})^2 + a_3Q_{ch} + a_4Q_{ch}^2 + a_5(T_{cw,o} - T_{chws})Q_{ch} \quad (60)$$

where  $a_0$ – $a_5$  represents the undetermined characteristic coefficient, which can be obtained through fitting and regression of the operation data.

Since adjusting the mass flow rate of the chilled water loop and cooling water loop of the condenser can change the operating conditions of the refrigerator, 229 groups of experiments were carried out by matching different flow rates. The experimental data is divided into a fitting data set and a validation data set, of which the validation set accounts for 20% of the total data. A three-dimensional nonlinear surface fitting method is selected and Figure 7 shows the results.

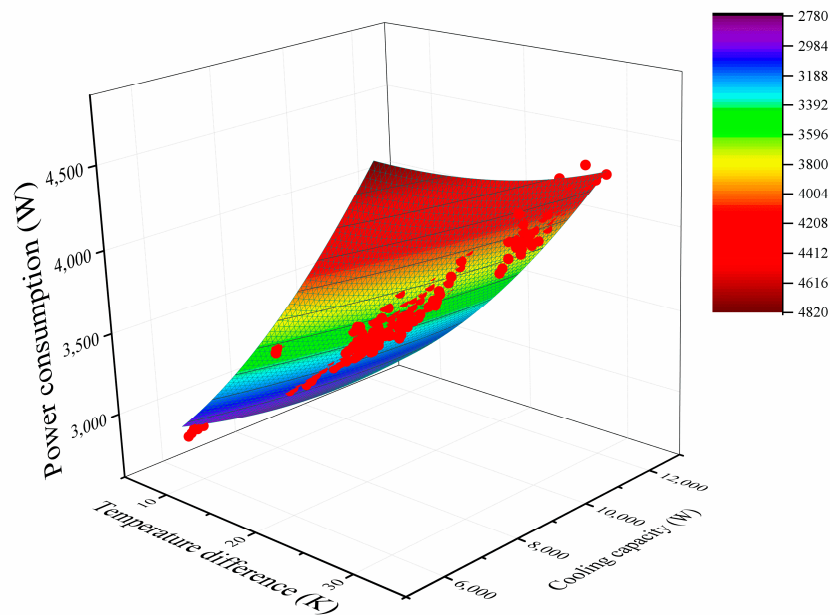


Figure 7. Fitting effect diagram.

Figure 8 shows the deviations between the validation group data and the fitting values. Table 6 shows the characteristic parameters, fitting similarity  $R^2$ , and the deviation between experimental data and fitting data. The fitting similarity  $R^2$  is 0.984, and the maximum deviation is 2.7%. Therefore, the prediction model can reflect the operating characteristics of the refrigerator commendably.

Table 6. Performance parameters of refrigerator,  $R^2$  and  $\delta_{max}$ .

$a_0$	$a_1$	$a_2$	$a_3$	$a_4$	$a_5$	$R^2$	$\delta_{max}$
2986.3	53.9	1.14	−0.132	$7.588 \times 10^{-6}$	−0.00248	0.984	2.7%

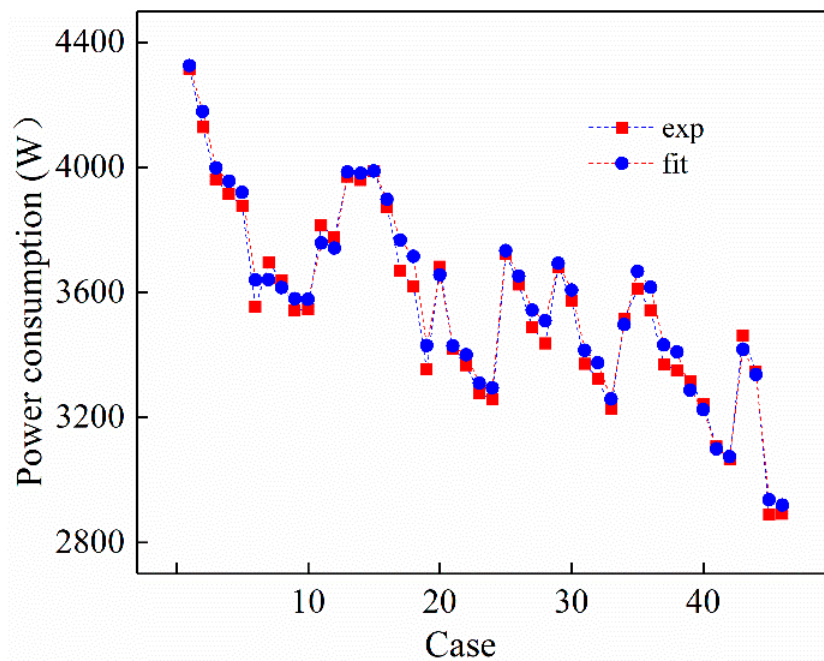


Figure 8. Comparison between fitting value and experimental value.

### 3.4. Artificial Neural Network Model for Predicting Thermal Conductivity of Heat Exchangers

The thermal conductivity ( $kA$ ) of heat exchangers reflects its heat transfer capacity and is one of the important parameters for solving heat transfer models. In a fixed heat exchanger,  $kA$  is mostly related to the fluid flow rate on the cold and hot sides. Assuming that the thermophysical properties of the fluid remain unchanged, there is a complex nonlinear relationship between  $kA$  and the mass flow rate of the cold and hot side fluid. Based on the experimental data, this paper establishes a neural network model with the flow rate of cold and hot side fluid of the heat exchanger as the input variable and  $kA$  as the output variable.

Firstly, 140 sets of experimental data were divided into training, testing, and validation sets in a ratio of 7:1.5:1.5. The two neurons in the input layer are the mass flow rates of hot and cold fluids, and one neuron in the output layer is  $kA$  of the heat exchanger. Set the hidden layer to 9 layers. Normalization and denormalization of the dataset can improve training accuracy. The Levenberg–Marquardt method was used for training, and the model was trained multiple times to achieve optimal results. Following a similar method, neural network modeling was performed on other heat exchangers. Table 7 shows the  $R^2$  of heat exchangers.

Table 7.  $R^2$  of heat exchangers.

Parameters	$(kA)_{a1}$	$(kA)_{a2}$	$(kA)_{a3}$	$(kA)_{a4}$	$(kA)_{a5}$	$(kA)_{a6}$	$(kA)_m$	$(kA)_{ct}$
$R^2$	0.964	0.946	0.971	0.938	0.985	0.967	0.953	0.943

### 3.5. Objective Function and Optimization Model

This research aims to optimize the system with the lowest total energy consumption, which is

$$\min P_{total} = \min(P_{re} + P_{pump}), j = 1, 2, \dots, 6 \tag{61}$$

$$P_{pump} = \sum_{j=1}^6 P_{aj} + P_{ch1} + P_{ch3} + P_m + P_{ct}, j = 1, 2, \dots, 6 \tag{62}$$

where  $P_{\text{pump}}$  is the total pump power of all power components,  $P_{aj}(j = 1, 2, \dots, 10)$  is the power of the  $j$ -th ACL fan.  $P_{ch1}$  is the power of the No.1 CHWC pump,  $P_{ch3}$  is the power of the No.3 CHWC pump,  $P_m$  is the power of the ICC pump, and  $P_{ct}$  is the power of the ACTC pump, their expressions are

$$P_{aj} = m_{aaj}gH_{aj}, j= 1, 2, \dots, 6 \tag{63}$$

$$P_{ch1} = m_{01}gH_{ch1} \tag{64}$$

$$P_{ch3} = m_{04}gH_{ch3} \tag{65}$$

$$P_{ct} = m_{ct}gH_{ct} \tag{66}$$

$$P_m = m_mgH_{ct} \tag{67}$$

where  $g$  is the acceleration of gravity.  $H_{aj}$  is the pressure head of the  $j$ -th ACL fan.  $H_{ch1}$  is the pressure head of the No. 1 CHWC pump,  $H_{ch3}$  is the pressure head of the No. 3 CHWC pump,  $H_m$  is the pressure head of the ICC pump, and  $H_{ct}$  is the pressure head of the ACTC pump.

For this refrigeration and ventilation system experimental platform, when the system structure remains unchanged, that is, when the flow resistance characteristic parameters of each circulation circuit remain unchanged, optimizing the working frequency of each power component under given heat load conditions can make the refrigerator and even the system operate in the optimal working state, thereby minimizing the total energy consumption of the system (61). Therefore, taking the total energy consumption of the heat exchange system as the optimization goal, combined with the overall heat transfer constraints (16) and (27) and flow constraints of the system (39)–(54), the Lagrange multiplier method is used for optimization calculation. The Lagrange function constructed is as follows:

$$\begin{aligned}
 F = & P_{re} + \sum_{j=1}^6 P_{aj} + P_{ch1} + P_{ch3} + P_m + P_{ct} + P_{ch} \\
 & + lamda_1(T_{aa1,i} - T_{chws} - R_{a1}Q_{a1}) \\
 & + lamda_2(T_{aa2,i} - T_{chws} - R_{a2}Q_{a2}) \\
 & + lamda_3(T_{aa3,i} - T_{chws} - R_{a3}Q_{a3}) \\
 & + lamda_4(T_{aa4,i} - T_{chws} - R_{a4}Q_{a4}) \\
 & + lamda_5(T_{aa5,i} - T_{chws} - R_{a5}Q_{a5}) \\
 & + lamda_6(T_{aa6,i} - T_{chws} - R_{a6}Q_{a6}) \\
 & + lamda_7(T_{ct,i} - T_{cw,\rho} - Q_cR_{ct} + \epsilon_{ct} - Q_cR_m) \\
 & + lamda_8(d_0m_0^2 + d_{01}m_{01}^2 + d_{02}m_{02}^2 + d_3m_{aw3}^2 + d_{03}m_{03}^2 - (d_0m_0^2 + d_{01}m_{01}^2 + d_{02}m_{02}^2 + d_5m_{aw5}^2)) \\
 & + lamda_9(d_0m_0^2 + d_{01}m_{01}^2 + d_1m_{aw1}^2 + d_{03}m_{03}^2 - (d_0m_0^2 + d_{01}m_{01}^2 + d_{02}m_{02}^2 + d_5m_{aw5}^2)) \\
 & + lamda_{10}(d_0m_0^2 + d_{04}m_{04}^2 + d_{05}m_{05}^2 + d_4m_{aw4}^2 + d_{06}m_{06}^2 - (d_0m_0^2 + d_{04}m_{04}^2 + d_{05}m_{05}^2 + d_6m_{aw6}^2)) \\
 & + lamda_{11}(d_0m_0^2 + d_{04}m_{04}^2 + d_2m_{aw2}^2 + d_{06}m_{06}^2 - (d_0m_0^2 + d_{04}m_{04}^2 + d_{05}m_{05}^2 + d_6m_{aw6}^2)) j= 1, 2, \dots, 6
 \end{aligned} \tag{68}$$

where  $lamda_k(k = 1, 2, \dots, 10)$  are Lagrange multipliers.

By combining Equations (55)–(59) and (62)–(67) with the Lagrange function (68) and making the partial derivatives of the equation with respect to  $\omega_{aaj}$ ,  $\omega_m$ ,  $\omega_{ct}$ ,  $m_{awj}$ , and  $lamda_k$  equal to zero, the following optimization equations can be obtained:

$$\frac{\partial F}{\partial X_n} = 0, X_n \in \{\omega_{aaj}, \omega_m, \omega_{ct}, m_{awj}, lamda_k\} j= 1, 2, \dots, 6, k= 1, 2, \dots, 11 \tag{69}$$

The equation group 64 contains 25 equations and 25 unknowns. Solving the equation group can obtain the operating frequencies of each power component with the lowest total power consumption of the system. Figure 9 shows the flowchart of the optimization solution. Firstly, the boundary conditions of the system, such as temperature, heat transfer, and other parameters, are given. Then, initial values are assigned to the solving objective.



**Table 9.** Optimal frequencies optimization of system power components (Hz).

	$\omega_{a1}$	$\omega_{a2}$	$\omega_{a3}$	$\omega_{a4}$	$\omega_{a5}$	$\omega_{a6}$	$\omega_{c1}$	$\omega_{c3}$	$\omega_m$	$\omega_{ct}$
Opt.	36.9	25.0	26.0	44.2	26.8	36.2	27.4	30.2	45.9	27.9

Table 10 shows the variations of the power consumption and heat transfer rate before and after optimization. After optimization, the total power consumption of all pumps ( $P_{\text{pump}}$ ) decreases by 39.1%, the energy consumption of the refrigerator saves by 11.4%, and the total power consumption of the system ( $P_t$ ) drops by 16.5%. Due to the decrease in power consumption of the refrigerator, according to Formula (6), the total heat transfer rate of the system decreases by 3.35%, which slows down the cooling pressure of the intermediate heat exchanger and air-cooling tower. The COP of the refrigerator increases by 11.6%.

**Table 10.** Change of system power consumption and heat transfer rate.

	$P_{\text{pump}}$ (W)	$P_{\text{re}}$ (W)	$P_t$ (W)	COP	$Q_c$ (W)
Pre.	816.5	3600	4416.5	2.52	12,700
Opt.	497.3	3193.1	3690.4	2.85	12,293.1
Deviation	−39.1%	−11.4%	−16.5%	11.6%	−3.3%

The optimal frequencies of power components are inputted into the experimental platform to verify the accuracy of the optimization by comparing the experimental and optimized values. Recording the data after the stable operation of the experimental platform. Table 11 shows that the maximum deviation of the thermal conductivity is 7.7%, which is within the allowable range of error.

**Table 11.** Heat conductance of heat exchanger (W/K).

	$(kA)_{a1}$	$(kA)_{a2}$	$(kA)_{a3}$	$(kA)_{a4}$	$(kA)_{a5}$	$(kA)_{a6}$	$(kA)_m$	$(kA)_{ct}$
Opt.	88.8	89.2	98.0	108.8	99.5	158.1	1667.9	5612.9
Exp.	82.6	93.8	95.4	102.4	91.9	149.5	1731.4	5294.4
Deviation	7.5%	5.2%	2.7%	5.9%	7.7%	5.5%	3.7%	5.7%

Table 12 shows the deviations of heat transfer rate at each node and energy consumption of the refrigerator. It can be seen that the maximum deviation of the heat transfer rate is 8.8%, and the error in the heat transfer rate at each node is within an acceptable range. The error in energy consumption of the refrigerator is 2.8%, which validates the optimization model.

**Table 12.** Heat transfer rate and energy consumption of the refrigerator (W).

	$Q_{a1}$	$Q_{a2}$	$Q_{a3}$	$Q_{a4}$	$Q_{a5}$	$Q_{a6}$	$Q_{ch}$	$P_{re}$	$Q_c$
Opt.	1200	1200	1400	1600	1400	2300	9100	3193.1	12,293.1
Exp.	1095	1240	1278	1625	1312	2464	8820	3285.0	13,393.0
Deviation	8.8%	3.4%	8.8%	1.6%	6.3%	7.2%	3.1%	2.8%	8.3%

#### 4.2. The Variation Law of Optimal Operating Parameters under Variable Heat Load

The change in heat transfer rate of the air cooler affects the total heat transfer rate of the system. This section discusses the optimal frequency of the system under different heat transfer rates by changing the heat transfer rate of the air cooler. The No. 1, No. 3, and No. 5 air coolers belong to a chilled water circuit, which is connected in parallel with the chilled water circuits of the No. 2, No. 4, and No. 6 air coolers. So, the No. 5 and No. 6 air coolers were selected for discussion.

Firstly, the heat transfer rate of the No. 5 air cooler is set from 1250 to 1600 W, and the total heat transfer rate of the system changes accordingly. The trends of the optimized operating frequency of the system power components are shown in Figure 10. It can be seen that the change in the heat exchange rate of the No. 5 air cooler has the greatest impact on the No. 5 fan, with its frequency increasing from 14.2 Hz to 32.4 Hz, followed by the frequency of the No. 1 chilled water pump increasing from 17.3 Hz to 32.3 Hz. In other words, due to the increase in heat transfer rate of the air cooler, the flow rate on both sides needs to increase to match the heat transfer rate of the air cooler. At the same time, the frequency of the intermediate cooling circuit pump and the cooling tower circuit pump increases to improve the heat transfer capacity of the system.

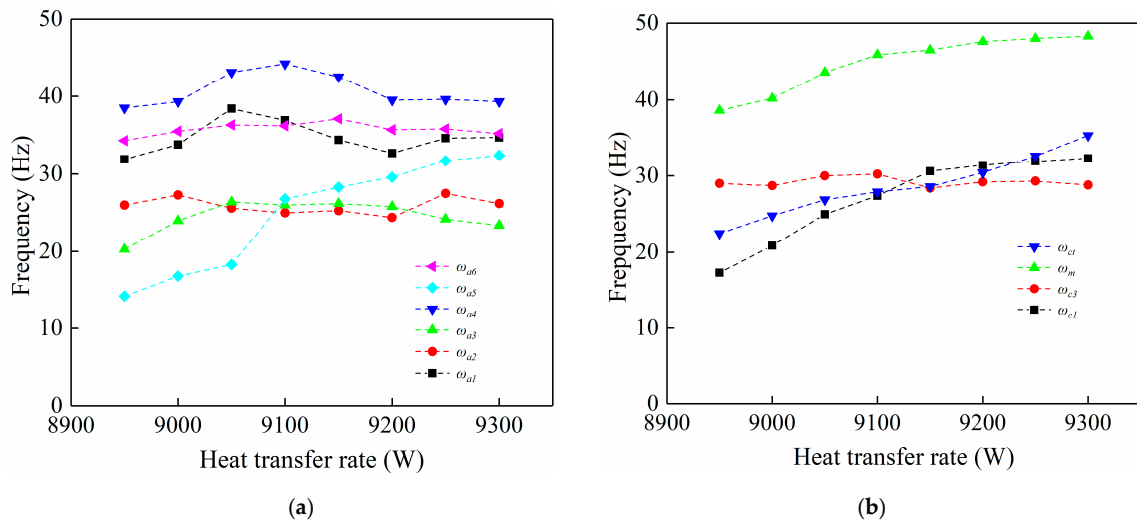


Figure 10. Optimal frequency of system power components under different heat loads. (a) Frequency variation of 6 air coolers. (b) Frequency variation of each circulating water pump.

By changing the heat transfer rate of the No. 6 air cooler, the trends of the optimized operating frequency of the system power components are shown in Figure 11. It can be seen that with the change in heat transfer rate of the No. 6 air cooler, the impact of the No. 6 fan is the greatest, increasing from 30.4 Hz to 44.3 Hz, followed by the frequency of No. 3 chilled water pump increasing from 28.9 Hz to 34.4 Hz. The optimized pattern is similar to the optimization conclusion of the No. 5 air cooler. The frequency variation of other pumps has no obvious pattern.

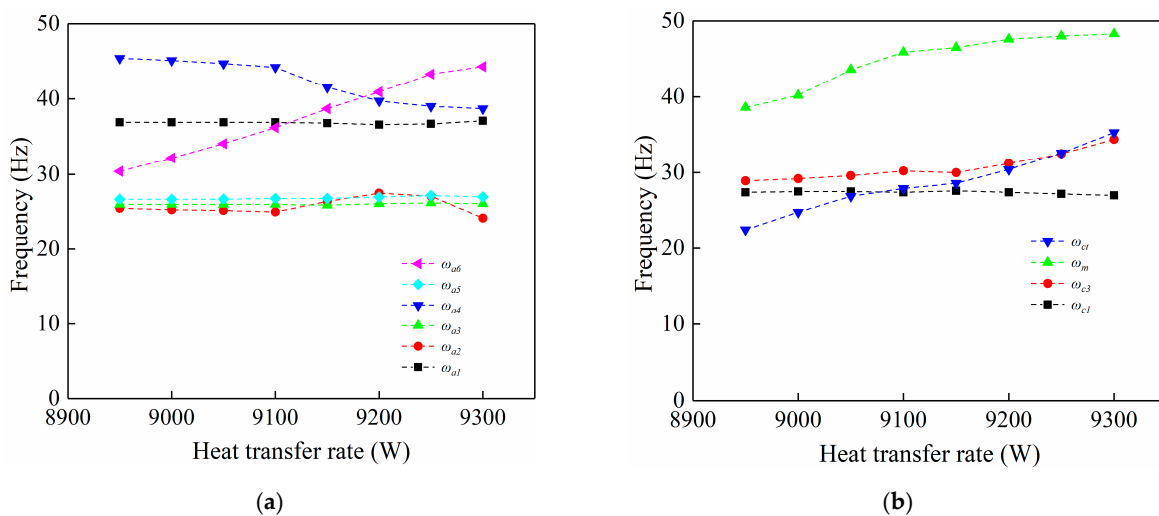


Figure 11. Optimal frequency of system power components under different heat loads. (a) Frequency variation of 6 air coolers. (b) Frequency variation of each circulating water pump.

## 5. Conclusions

In this study, a refrigeration and ventilation experimental platform as well as its operation optimization were carried out to solve the serious thermal damage problems in deep metal mines. The heat current method is used to analyze the heat transfer process of the system. With the goal of minimizing the total power consumption of the system, combining the energy consumption model of refrigeration established the optimization model.

The optimization results show that the total power consumption of such power components as fans and pumps was reduced by 39.1%, the power consumption of the refrigerator saved by 11.4%, and the total energy consumption of the system saved by 16.5%. Meanwhile, the total heat transfer rate of the system was reduced by 3.35%, and the COP of the refrigerator was reduced by 11.6%. The optimization results significantly improve the operating efficiency of the refrigerator while reducing the cooling load of the heat exchanger. The comparison between the optimized value and the experimental value shows that the maximum deviation of heat transfer rate is 8.8%, the maximum deviation of thermal conductivity is 7.7%, and the maximum deviation of energy consumption of the refrigerator is 2.8%, all of which are within the allowable range of error. This optimization method can reduce systematic energy consumption and improve the operating efficiency of the refrigerator while meeting the cooling load of the system. The modeling and optimization ideas have important guiding significance for related systems, and the optimization results have played a role in energy conservation and consumption reduction.

**Author Contributions:** Conceptualization, W.W., W.S. and Z.C. (Zheng Cui); Methodology, W.W., S.W., J.L. and Z.C. (Zhuoqun Cao); Formal analysis, W.W. and K.S.; Investigation, Y.L.; Resources, K.S.; Data curation, W.W. and Z.C. (Zhuoqun Cao); Writing—Original draft, W.W.; Writing—Review & editing, W.S.; Supervision, W.S. and Z.C. (Zheng Cui); Funding acquisition, W.S. and Z.C. (Zheng Cui). All authors have read and agreed to the published version of the manuscript.

**Funding:** This work was supported by the Natural Science Foundation of Shandong Province (No. ZR2021QE033), and the Major Science and Technological Innovation Projects of Shandong Province (Grand No. 2019SDZY05).

**Data Availability Statement:** The data are not publicly available due to restrictions eg privacy or ethical.

**Conflicts of Interest:** The authors declare no conflict of interest.

## Nomenclature

<i>a</i>	Performance characteristic parameters of power components (variable frequency pump or variable frequency fan)
<i>A</i>	Heat transfer area, m <sup>2</sup>
<i>ACTC</i>	Air-cooling tower circuit
<i>CHWC</i>	Chilled water circuit
<i>CAL</i>	Cooling airline
<i>COP</i>	The coefficient of performance of the refrigerator
<i>c<sub>p</sub></i>	Constant pressure specific heat, (J/(kg·K))
<i>H</i>	Pressure head, m
<i>ICC</i>	intermediate cooling circuit
<i>g</i>	Acceleration of gravity, m/s <sup>2</sup>
<i>G</i>	Entransy, J·K; Heat capacity flow, W/K
<i>k</i>	Heat transfer coefficient, W/(K·m <sup>2</sup> )
<i>kA</i>	Thermal conductance, W/K
<i>KCL</i>	Kirchhoff's circuit law
<i>KVL</i>	Kirchhoff's voltage law
<i>lamda</i>	Lagrange multiplier
<i>m</i>	Mass flow rate, kg/s
<i>NTU</i>	Number of heat transfer units

$\rho$	Density, kg/m <sup>3</sup>
$p$	Pressure, Pa
$P$	Power, W
$Q$	Heat transfer rate, W
$Q_a$	Heat transfer rate of air coolers, W
$Q_{ch}$	Total refrigeration capacity of the refrigerator, W
$Q_{ct}$	Heat transfer rate of air-cooling tower, W
$Q_m$	Heat transfer rate of the intermediate heat exchanger/total heat transfer rate of system, W
$R$	Equivalent thermal resistance, K/W
$R_g$	Entransy dissipation-based thermal resistance, K/W
$T$	Temperature, K or °C
$\Delta T_m$	Logarithm mean temperature difference, K
$U$	Uncertainty
$\omega$	Operating frequency of power components, Hz
$W$	Power consumption, W
$\delta$	Deviation
$\varepsilon$	Equivalent thermal potential difference
Subscripts	
$a$	Air
$c$	Condensation process; condenser
$cal$	Calculated value
$cr$	Refrigerant
$ch, chw$	Chilled water
$chws$	Chilled water supply
$chwr$	Chilled water return
$ct$	Air-cooling tower cooling circuit/air-cooling tower
$cw$	Cooling water
$cws$	Cooling water supply
$cwr$	Cooling water return
$e$	Evaporation process/evaporator
$exp$	Experimental value
$fit$	Fitting value
$h$	Hot side; hot fluid
$i$	Inlet
$m$	Intermediate cooling circuit/intermediate heat exchanger
$o$	Outlet
$re$	Refrigerator
$w$	Water

## References

- Xu, Y.; Li, Z.; Chen, Y.; Jia, M.; Zhang, M.; Li, R. Synergetic mining of geothermal energy in deep mines: An innovative method for heat hazard control. *Appl. Therm. Eng.* **2022**, *210*, 118398. [\[CrossRef\]](#)
- Crawford, J.A.; Joubert, H.P.R.; Mathews, M.J.; Kleingeld, M. Optimised dynamic control philosophy for improved performance of mine cooling systems. *Appl. Therm. Eng.* **2019**, *150*, 50–60. [\[CrossRef\]](#)
- Xiaojie, Y.; Qiaoyun, H.; Jiewen, P.; Xiaowei, S.; Dinggui, H.; Chao, L. Progress of heat-hazard treatment in deep mines. *Min. Sci. Technol.* **2011**, *21*, 295–299. [\[CrossRef\]](#)
- He, M.-C. Application of HEMS cooling technology in deep mine heat hazard control. *Min. Sci. Technol.* **2009**, *19*, 269–275. [\[CrossRef\]](#)
- Niu, Y. Research on Thermal Energy Recycling Utilization in High Temperature Mines. *Procedia Eng.* **2015**, *121*, 389–395. [\[CrossRef\]](#)
- Li, Y.; Hu, H.; Sun, H.; Wu, C. Dynamic simulation model for three-wheel air-cycle refrigeration systems in civil aircrafts. *Int. J. Refrig.* **2023**, *145*, 353–365. [\[CrossRef\]](#)
- Sun, J.; Kuruganti, T.; Munk, J.; Dong, J.; Cui, B. Low global warming potential (GWP) refrigerant supermarket refrigeration system modeling and its application. *Int. J. Refrig.* **2021**, *126*, 195–209. [\[CrossRef\]](#)
- Li, Z.; Liang, K.; Chen, X.; Zhu, Z.; Zhu, Z.; Jiang, H. A comprehensive numerical model of a vapour compression refrigeration system equipped with a variable displacement compressor. *Appl. Therm. Eng.* **2022**, *204*, 117967. [\[CrossRef\]](#)

9. Tirmizi, S.A.; Gandhidasan, P.; Zubair, S.M. Performance analysis of a chilled water system with various pumping schemes. *Appl. Energy* **2012**, *100*, 238–248. [[CrossRef](#)]
10. Huh, J.-H.; Brandemuehl, M.J. Optimization of air-conditioning system operating strategies for hot and humid climates. *Energy Build.* **2008**, *40*, 1202–1213. [[CrossRef](#)]
11. Baakeem, S.S.; Orfi, J.; Alabdulkarem, A. Optimization of a multistage vapor-compression refrigeration system for various refrigerants. *Appl. Therm. Eng.* **2018**, *136*, 84–96. [[CrossRef](#)]
12. Zhao, L.; Cai, W.; Ding, X.; Chang, W. Model-based optimization for vapor compression refrigeration cycle. *Energy* **2013**, *55*, 392–402. [[CrossRef](#)]
13. Nunes, T.K.; Vargas, J.V.C.; Ordonez, J.C.; Shah, D.; Martinho, L.C.S. Modeling, simulation and optimization of a vapor compression refrigeration system dynamic and steady state response. *Appl. Energy* **2015**, *158*, 540–555. [[CrossRef](#)]
14. Chang, Y.-C.; Lin, J.-K.; Chuang, M.-H. Optimal chiller loading by genetic algorithm for reducing energy consumption. *Energy Build.* **2005**, *37*, 147–155. [[CrossRef](#)]
15. Adelekan, D.S.; Ohunakin, O.S.; Paul, B.S. Artificial intelligence models for refrigeration, air conditioning and heat pump systems. *Energy Rep.* **2022**, *8*, 8451–8466. [[CrossRef](#)]
16. Sanzana, M.R.; Maul, T.; Wong, J.Y.; Abdulrazic, M.O.M.; Yip, C.-C. Application of deep learning in facility management and maintenance for heating, ventilation, and air conditioning. *Autom. Constr.* **2022**, *141*, 104445. [[CrossRef](#)]
17. Wang, L.; Lee, E.W.M.; Yuen, R.K.K. A practical approach to chiller plants' optimisation. *Energy Build.* **2018**, *169*, 332–343. [[CrossRef](#)]
18. Chen, Q.; Fu, R.-H.; Xu, Y.-C. Electrical circuit analogy for heat transfer analysis and optimization in heat exchanger networks. *Appl. Energy* **2015**, *139*, 81–92. [[CrossRef](#)]
19. Shen, G.; Yuan, F.; Li, Y.; Liu, W. The energy flow method for modeling and optimization of Organic Rankine Cycle (ORC) systems. *Energy Convers. Manag.* **2019**, *199*, 111958. [[CrossRef](#)]
20. Chen, X.; Chen, Q.; Chen, H.; Xu, Y.-G.; Zhao, T.; Hu, K.; He, K.-L. Heat current method for analysis and optimization of heat recovery-based power generation systems. *Energy* **2019**, *189*, 116209. [[CrossRef](#)]
21. Wang, Y.; Zhang, Y.; Hao, J.; Pan, H.; Ni, Y.; Di, J.; Ge, Z.; Chen, Q.; Guo, M. Modeling and operation optimization of an integrated ground source heat pump and solar PVT system based on heat current method. *Sol. Energy* **2021**, *218*, 492–502. [[CrossRef](#)]
22. Shao, W.; Chen, Q.; Zhang, M.Q. Operation optimization of variable frequency pumps in compound series-parallel heat transfer systems based on the power flow method. *Energy Sci. Eng.* **2018**, *6*, 385–396. [[CrossRef](#)]
23. Li, X.; Chen, Q.; Hao, J.-H.; Chen, X.; He, K.-L. Heat current method for analysis and optimization of a refrigeration system for aircraft environmental control system. *Int. J. Refrig.* **2019**, *106*, 163–180. [[CrossRef](#)]
24. Chen, Q.; Wang, Y.-F.; Zhang, M.-Q. Optimization strategies of heat transfer systems with consideration of heat transfer and flow resistance. *Int. J. Heat Mass Transf.* **2017**, *112*, 137–146. [[CrossRef](#)]
25. Zhao, T.; Liu, D.; Chen, Q. A collaborative optimization method for heat transfer systems based on the heat current method and entransy dissipation extremum principle. *Appl. Therm. Eng.* **2019**, *146*, 635–647. [[CrossRef](#)]
26. Bergman, T.L.; Lavine, A.S.; Incropera, F.P. Fundamentals of Heat and Mass Transfer. *Staff. Gen. Res. Pap.* **1996**, *27*, 139–162.
27. Chen, Q.; Hao, J.-H.; Zhao, T. An alternative energy flow model for analysis and optimization of heat transfer systems. *Int. J. Heat Mass Transf.* **2017**, *108*, 712–720. [[CrossRef](#)]
28. Zhao, T.; Chen, X.; He, K.-L.; Chen, Q. A standardized modeling strategy for heat current method-based analysis and simulation of thermal systems. *Energy* **2021**, *217*, 119403. [[CrossRef](#)]
29. Chen, Q.; Hao, J. Heat Current Method for Analysis and Optimization of Thermal System. Science Press: Beijing, China, 2020.
30. Yang, Z.; Borsting, H. Energy Efficient Control of a Boosting System with Multiple Variable-Speed Pumps in Parallel. In Proceedings of the IEEE Conference on Decision & Control, Atlanta, GA, USA, 15–17 December 2010.
31. Rishel, J.; Durkin, T.; Kincaid, B. *HVAC Pump Handbook*; McGraw Hill Book, Co.: New York, NY, USA, 1996.
32. Munson, B.R. *WIE Fundamentals of Fluid Mechanics*, 4th ed.; Wiley: Hoboken, NJ, USA, 2021.
33. Handbook, A. *ASHRAE Handbook-HVAC Applications (SI)*; ASHRAE Inc.: Atlanta, GA, USA, 2011.

**Disclaimer/Publisher's Note:** The statements, opinions and data contained in all publications are solely those of the individual author(s) and contributor(s) and not of MDPI and/or the editor(s). MDPI and/or the editor(s) disclaim responsibility for any injury to people or property resulting from any ideas, methods, instructions or products referred to in the content.